Phase-Shift Calculation of High-Energy Electron Scattering*

D. R. YENNIE, D. G. RAVENHALL, AND R. N. WILSON
Department of Physics, Stanford University, Stanford, California
(Received March 22, 1954)

The details of a phase-shift calculation of high-energy electron scattering by nuclei are given, together with some preliminary results. A new method for summing the Legendre series for the Coulomb scattering amplitude is described. The results indicate that the first Born approximation does not give cross sections accurate enough for a reliable interpretation of the experiments. From a comparison of the few theoretical cross sections already obtained with the experiments in gold at 125 Mev, very tentative conclusions about the nuclear charge distribution are drawn. It is pointed out that an analysis of results at two or more energies will be a much more sensitive test of possible charge distributions.

I. INTRODUCTION

EXPERIMENTS on the elastic scattering of high-energy electrons by nuclei carried out by Hofstadter, Fechter, and McIntyre,[1] and by Pidd, Hammer, and Raka[2] exhibit clearly the finite extension of the nuclear charge distributions. Analyses of the results of Hofstadter's group by Hofstadter *et al.*[1] and by Schiff,[3] using the first Born approximation, led to the tentative conclusion that the charge distribution was peaked at the center of the nucleus, tapering gradually towards the edge. In view of the fact that the Born approximation is not accurate for heavy elements, we have carried out a phase-shift analysis of the process. A brief report of preliminary results has already been made.[4] We wish in this paper to give an account of our methods and of the trend of our results. Our calculations have been of an exploratory nature, with a view to fitting the experimental data at 125 Mev,[1] and we can as yet draw no definite conclusions about nuclear charge distributions. To do so will require a thorough examination of the new and more accurate results of Hofstadter's group at several energies, and we hope to report on this in the near future.

The literature on electron scattering by nuclei is very extensive, and we shall not survey all of it here. That relating to estimates of the effect of the finite nuclear size using the first Born approximation has been summarized in Schiff's paper.[3] Phase-shift analyses of this process for the energy region where only one Coulomb phase shift is modified by the finite nuclear size have been made in papers by Elton,[5] Acheson,[6] and Feshbach.[7] Bitter and Feshbach[8] showed that experiments in this region can measure only one parameter of the nuclear charge distribution, namely its root-mean-square radius. Until very recently the only calculation for an energy high enough to require the modification of several Coulomb phases, thus yielding a cross section characteristic of the particular shape of the nuclear charge distribution, has been that of Parzen,[9] but unfortunately his results are not correct.[10] Other calculations in this energy range have now been made by E. Baranger,[11] and Brenner, Brown, and Elton.[12]

The model we use is the Dirac equation for an electron in the electrostatic potential of a static, spherically symmetric charge distribution. The cross section is obtained by a numerical calculation of the phase shift of each partial wave. It is unfortunate that the complexity of the calculation tends to obscure the relationship between the details of the charge distributions and of the corresponding cross sections. A method which avoided the decomposition into partial waves might give more insight into the process. We do not take into account the interaction of the electron with nuclear magnetic or electric quadrupole moments, or the effect of nuclear excitation. Calculations by Schiff[13] using the first Born approximation suggest that the first is not important at the energies under consideration, and that the other two are small except with particular elements at large angles. We also ignore quantum electrodynamic radiative corrections. Schwinger's analysis[14] predicts a very small change in the angular dependence of the differential cross section (of the order of one or two percent), but this also is on the basis of the first Born approximation.

In Part II we give an account of scattering theory for the Dirac equation, neglecting the mass term, as is justified at high energies. As an excuse for presenting such a well-studied topic again, we claim that our version, in which the omission of the mass term is made before the reduction to partial waves, is simpler and more transparent than the usual treatment. The only

* Supported in part by the U. S. Office of Scientific Research, Air Research and Development Command.

[1] Hofstadter, Fechter, and McIntyre, Phys. Rev. **91**, 422 (1953); **92**, 978 (1953).
[2] Pidd, Hammer, and Raka, Phys. Rev. **92**, 436 (1953).
[3] L. I. Schiff, Phys. Rev. **92**, 988 (1953).
[4] Yennie, Wilson, and Ravenhall, Phys. Rev. **92**, 1325 (1953).
[5] L. R. B. Elton, Phys. Rev. **79**, 412 (1950); Proc. Phys. Soc. (London) **A63**, 1115 (1950); **A65**, 481 (1952); **A66**, 806 (1953).
[6] L. K. Acheson, Phys. Rev. **82**, 488 (1951).
[7] H. Feshbach, Phys. Rev. **84**, 1206 (1951).
[8] F. Bitter and H. Feshbach, Phys. Rev. **92**, 837 (1953).
[9] G. Parzen, Phys. Rev. **80**, 355 (1950).
[10] An error was discovered by E. Baranger (see reference 11).
[11] E. Baranger, Phys. Rev. **93**, 1127 (1954). We wish to thank Mrs. Baranger for an interesting discussion of her work and ours.
[12] Brenner, Brown, and Elton (to be published). We thank Dr. Brown for communicating these results to us prior to their publication.
[13] Reference 3, and L. I. Schiff (private communication).
[14] J. Schwinger, Phys. Rev. **75**, 898 (1949).

new feature is our summing of the series for the Coulomb scattering amplitude. It is with reluctance that we introduce a new notation for the quantum number characterizing the partial wave. We think it clearer and more consistent to use j than the k, n, and l of previous authors, since j^2, the familiar total angular momentum operator, is actually diagonal in the representation used.

The results are presented in Part III, together with a brief comparison with the work of other authors, and the qualitative conclusions that we feel able to draw at present.

II. THEORY

1. Dirac Equation at High Energies

We shall be concerned with the scattering of electrons at very high energies ($E>50\ mc^2$). We then expect that it should be possible to neglect the rest energy of the electron in comparison with its total energy. It is physically obvious that such an approximation should not introduce any qualitative changes into the scattering properties of the electron, and in fact the only quantitative changes introduced are of relative order (m^2c^4/E^2).[6,12]

In the Dirac equation,

$$(\boldsymbol{\alpha}\cdot\mathbf{p}c+\beta mc^2+V)\psi=E\psi, \tag{1}$$

we choose a representation for the Dirac matrices which will facilitate neglecting the mass term:

$$\alpha_i=\rho_3\sigma_i, \quad \beta=\rho_1.[15] \tag{2}$$

If we write ϕ and χ for two two-component wave functions, the Dirac equation can then be written

$$\begin{aligned}(\boldsymbol{\sigma}\cdot\mathbf{p}c+V-E)\phi&=-mc^2\chi, \\ (-\boldsymbol{\sigma}\cdot\mathbf{p}c+V-E)\chi&=-mc^2\phi.\end{aligned} \tag{3}$$

Neglecting the mass, we obtain two sets of uncoupled equations:

$$(\boldsymbol{\sigma}\cdot\mathbf{p}c+V-E)\phi=0, \tag{4a}$$

$$(-\boldsymbol{\sigma}\cdot\mathbf{p}c+V-E)\chi=0. \tag{4b}$$

That such two-component equations should exist can be seen directly from the original Dirac equation (1) by noting that when the term involving β is neglected, the remaining three hypercomplex quantities α_i can be represented by two component σ matrices. Solutions of both (4a) and (4b) are needed, however, in order to have a complete set of states for Eq. (1).[16]

Consider plane wave solutions of Eqs. (4a) and (4b) in the absence of a potential:

$$\begin{aligned}\phi&=u\exp(i\mathbf{k}\cdot\mathbf{x}), \\ \chi&=v\exp(i\mathbf{k}\cdot\mathbf{x}),\end{aligned} \tag{5}$$

where

$$\begin{aligned}\boldsymbol{\sigma}\cdot(\hbar c\mathbf{k})u&=Eu, \\ \boldsymbol{\sigma}\cdot(\hbar c\mathbf{k})v&=-Ev.\end{aligned} \tag{6}$$

For a given $E(>0)$ and $\mathbf{k}$, these two solutions correspond to the two different spin states of the electron. Loosely speaking, for the first solution the spin is parallel to the momentum while for the second it is antiparallel. The normalized solutions of (6) are

$$\begin{aligned}u&=\begin{pmatrix}\cos\tfrac{1}{2}\theta \\ \sin\tfrac{1}{2}\theta\exp(i\varphi)\end{pmatrix}, \\ v&=\begin{pmatrix}-\sin\tfrac{1}{2}\theta\exp(-i\varphi) \\ \cos\tfrac{1}{2}\theta\end{pmatrix},\end{aligned} \tag{7}$$

where θ and φ are the polar angles specifying the direction of $\mathbf{k}$.

If we reintroduce the potential (which for the moment we assume has a finite extent), scattering states will have the asymptotic form[17]

$$\begin{aligned}\phi&\sim\begin{pmatrix}1\\0\end{pmatrix}e^{ikz}+r^{-1}f_1(\theta,\varphi)\begin{pmatrix}1\\ \tan\tfrac{1}{2}\theta\exp(i\varphi)\end{pmatrix}e^{ikr}, \\ \chi&\sim\begin{pmatrix}0\\1\end{pmatrix}e^{ikz}+r^{-1}f_2(\theta,\varphi)\begin{pmatrix}-\tan\tfrac{1}{2}\theta\exp(-i\varphi)\\ 1\end{pmatrix}e^{ikr}.\end{aligned} \tag{8}$$

It is easily seen that for a spherically symmetric potential the scattering in a given direction will be the same for both spin orientations.[18] In the following, we will therefore restrict our attention to Eq. (4a).

2. Scattering Theory of the Dirac Equation at High Energies

Any solution of Eq. (4a) can be decomposed into partial waves characterized by the total angular momentum and its z component:

$$\phi=\sum a_{jm}\phi_{jm}, \tag{9}$$

with

$$J^2\phi_{jm}=j(j+1)\hbar^2\phi_{jm}, \tag{10}$$

[15] P. A. M. Dirac, *The Principles of Quantum Mechanics* (Oxford University Press, Oxford, 1947), third edition, p. 256.

[16] A discussion of the relation between our analysis and that of previous authors is given in the Appendix.

[17] Acheson (see reference 6) has already shown that the two components of the scattered wave differ by only a factor $\tan\frac{1}{2}\theta\exp(i\varphi)$. His proof is based on relationships between spherical harmonics occurring in the expansions of the components. Our derivation gives the underlying reason for this.

[18] This may be seen as follows: If $\phi(\mathbf{x})$ is a solution of (4a), then $\chi(\mathbf{x})=\phi(-\mathbf{x})$ is a solution of (4b). If the incident wave part of $\phi(\mathbf{x})$ is traveling in the positive z direction, the incident wave part of $\chi(\mathbf{x})$ is traveling in the minus z direction. If now we rotate the second solution through 180° about the x axis, we have both incident waves traveling in the positive z direction and the intensity of the scattered waves in a given direction is the same for both solutions. Further analysis along this line shows that when we consider the scattering of electrons from randomly oriented nonsymmetric nuclei there can be no polarization of the scattered electrons; this refers only to static moments, of course. At lower energies where the mass cannot be neglected, polarization in scattering by a spherically symmetric potential is possible.

and

$$J_z\phi_{jm}=m\hbar\phi_{jm}, \tag{11}$$

where

$$\mathbf{J}=\mathbf{r}\times\mathbf{p}+\tfrac{1}{2}\boldsymbol{\sigma}\hbar.$$

For a plane-wave incident in the z direction

$$J_z\begin{pmatrix}1\\0\end{pmatrix}e^{ikz}=\tfrac{1}{2}\hbar\begin{pmatrix}1\\0\end{pmatrix}e^{ikz}, \tag{12}$$

so that we need be concerned only with the states $\phi_{j,\frac{1}{2}}$. The spin-angular parts of these states have the forms

$$\chi_j{}^1=\begin{pmatrix}(j+\frac{1}{2})P_{j-\frac{1}{2}}(\cos\theta)\\-P_{j-\frac{1}{2}}{}^1(\cos\theta)\exp(i\varphi)\end{pmatrix},$$
$$\chi_j{}^2=\begin{pmatrix}(j+\frac{1}{2})P_{j+\frac{1}{2}}(\cos\theta)\\P_{j+\frac{1}{2}}{}^1(\cos\theta)\exp(i\varphi)\end{pmatrix}. \tag{13}$$

The partial wave solutions of (4a) then take the form

$$\phi_{j,\frac{1}{2}}=r^{-1}[G_j(r)\chi_j{}^1+iF_j(r)\chi_j{}^2]. \tag{14}$$

In deriving the equations satisfied by F_j and G_j, the following identities are useful:

$$\boldsymbol{\sigma}\cdot\mathbf{L}\chi_j{}^1=\hbar(j-\tfrac{1}{2})\chi_j{}^1,$$
$$\boldsymbol{\sigma}\cdot\mathbf{L}\chi_j{}^2=-\hbar(j+\tfrac{3}{2})\chi_j{}^2, \tag{15}$$

$$\boldsymbol{\sigma}\cdot\mathbf{r}\chi_j{}^1=r\chi_j{}^2,$$
$$\boldsymbol{\sigma}\cdot\mathbf{r}\chi_j{}^2=r\chi_j{}^1, \tag{16}$$

$$\boldsymbol{\sigma}\cdot\mathbf{p}=r^{-2}(\boldsymbol{\sigma}\cdot\mathbf{r})(\mathbf{r}\cdot\mathbf{p})+ir^{-2}(\boldsymbol{\sigma}\cdot\mathbf{r})(\boldsymbol{\sigma}\cdot\mathbf{L}). \tag{17}$$

It is then easily found that[16]

$$\frac{dG_j}{dr}-\frac{(j+\frac{1}{2})}{r}G_j+\frac{(E-V)}{\hbar c}F_j=0,$$
$$\frac{dF_j}{dr}+\frac{(j+\frac{1}{2})}{r}F_j-\frac{(E-V)}{\hbar c}G_j=0. \tag{18}$$

It is convenient to handle these equations in dimensionless form. We therefore set

$$x=kr \tag{19}$$

and

$$v=V/E, \tag{20}$$

where

$$k=E/\hbar c.$$

Then

$$\frac{dG_j}{dx}-\frac{(j+\frac{1}{2})}{x}G_j+(1-v)F_j=0,$$
$$\frac{dF_j}{dx}+\frac{(j+\frac{1}{2})}{x}F_j-(1-v)G_j=0. \tag{21}$$

For use in the scattering calculation, we need those solutions of Eq. (21) which are regular at the origin.

We shall next review briefly the standard scattering theory for the non-Coulomb case, and finally modify the results thus obtained to take into account the peculiar nature of the Coulomb field. At large distances we expect to find an asymptotic solution of the form

$$\phi\sim\begin{pmatrix}1\\0\end{pmatrix}e^{ix\cos\theta}+x^{-1}kf(\theta)\begin{pmatrix}1\\\tan\frac{1}{2}\theta\exp(i\varphi)\end{pmatrix}e^{ix}$$
$$=\phi_{\text{inc}}+\phi_{\text{scatt}}. \tag{22}$$

The differential cross section is then given by

$$d\sigma/d\Omega=|f|^2(1+\tan^2\tfrac{1}{2}\theta)=\sec^2\tfrac{1}{2}\theta|f|^2. \tag{23}$$

Using the well-known expansion of plane waves,[19] we may express the incident wave as a sum of partial waves of the form (14):

$$\phi_{\text{inc}}=\sum_{j-\frac{1}{2}=0}^{\infty}\left(\frac{\pi}{2x}\right)^{\frac{1}{2}}i^{j-\frac{1}{2}}[J_j\chi_j{}^1+iJ_{j+1}\chi_j{}^2]. \tag{24}$$

The total wave, determined by the condition that its incoming wave part is the same as that of (24), is

$$\phi=\sum_{j-\frac{1}{2}=0}^{\infty}x^{-1}i^{j-\frac{1}{2}}e^{i\eta_j}[G_j\chi_j{}^1+iF_j\chi_j{}^2]. \tag{25}$$

The phase shifts η_j are determined by comparing the asymptotic radial functions in (25) with those in (24):

$$(\pi x/2)^{\frac{1}{2}}J_j(x)\sim\sin[x-\tfrac{1}{2}(j-\tfrac{1}{2})\pi],$$
$$G_j\sim\sin[x-\tfrac{1}{2}(j-\tfrac{1}{2})\pi+\eta_j]. \tag{26}$$

Combining Eqs. (25), (24), and (22) we find that the scattered wave is given by

$$f(\theta)=\frac{1}{2ik}\sum(e^{2i\eta_j}-1)(j+\tfrac{1}{2})(P_{j-\frac{1}{2}}+P_{j+\frac{1}{2}})$$
$$=\frac{1}{2ik}\sum e^{2i\eta_j}(j+\tfrac{1}{2})(P_{j-\frac{1}{2}}+P_{j+\frac{1}{2}}). \tag{27}$$

In going from the first form of Eq. (27) to the second, the terms dropped sum to zero, except in the forward direction ($\theta=0$).[20]

In the case of a Coulomb potential produced by an extended nucleus, the potential outside the nucleus takes the form

$$v=-\gamma/x,$$

where

$$\gamma=Ze^2/\hbar c. \tag{28}$$

The potential inside the charge distribution may be

[19] G. N. Watson, *Theory of Bessel Functions* (MacMillan Company, New York, 1946), revised edition, p. 128.

[20] This is best seen by putting $a_l{}^{(0)}=2l+1$ in Eq. (46) below. This gives $a_l{}^{(1)}=0$.

calculated by using the expression

$$-v(x)=4\pi\gamma x^{-1}\int_0^x \rho(x')x'^2dx'+4\pi\gamma\int_x^\infty \rho(x')x'dx', \quad (29)$$

where the dimensionless charge density ρ has the normalization

$$4\pi\int_0^\infty \rho x^2dx=1. \quad (30)$$

The results of the scattering theory must be modified slightly because of the long-range nature of the Coulomb potential. The proper asymptotic form of the scattered wave is

$$\phi_{\text{scatt}}=x^{-1}kf(\theta)\begin{pmatrix}1\\ \tan\tfrac{1}{2}\theta\exp(i\varphi)\end{pmatrix}e^{i(x+\gamma\ln 2x)}, \quad (31)$$

while the individual partial waves have the form

$$G_j(x)\sim\sin[x+\gamma\ln 2x-\tfrac{1}{2}(j-\tfrac{1}{2})\pi+\eta_j]. \quad (32)$$

The scattering amplitude $f(\theta)$ is still given by (27).

A complication of the Coulomb potential is that the phase shifts do not approach a limit as j increases. In fact, the magnitude of the phase shift increases roughly like $(\gamma\ln j)$ with increasing j. Nevertheless it is possible to sum the series (27).[21,22] An improved method for carrying out this summation is given in Sec. 4.

3. Method of Calculation

The computational problem is, of course, to integrate Eqs. (21) to determine the phase shifts, and from these to calculate the differential cross section. In this section we shall outline the method, and leave the computational details to Sec. 4 and the Appendix.

Unless we wish to use simple special expressions for the potential v, it is not easy to obtain the solutions of (21) in a closed form, or even as a power series expansion. Except for the pure Coulomb case (point charge), we therefore rely on numerical methods to integrate (21). These methods are presented in detail in the Appendix. It suffices to say here that in each step of the integration all the derivatives of F_j and G_j through the fourth are treated correctly. In future calculations we plan to include all derivatives through the sixth.

Starting with a regular solution obtained by a power series expansion about the origin, the differential equations (21) are integrated from $x=0.1$ to a point x_0 (the "fitting-on radius") which lies outside the nuclear charge distribution. At x_0 the pair of functions $G_j(x_0)$, $F_j(x_0)$ is fitted to two pairs of linearly independent Coulomb functions

$$\begin{aligned}G_j(x_0)&=C_jG_{j,R}(x_0)+D_jG_{j,I}(x_0),\\ F_j(x_0)&=C_jF_{j,R}(x_0)+D_jF_{j,I}(x_0).\end{aligned} \quad (33)$$

[21] N. F. Mott, Proc. Roy. Soc. (London) **A135**, 429 (1932).
[22] H. Feshbach, Phys. Rev. **88**, 295 (1953).

Here the subscript R (I) denotes a Coulomb function which is regular (irregular) at the origin. Both the regular and irregular Coulomb functions used here are given by power series expansions about the origin. The series used are given in the Appendix.

The asymptotic forms of the Coulomb functions are well known:

$$\begin{aligned}G_{j,R}&\sim\sin[x+\gamma\ln 2x-\tfrac{1}{2}(j-\tfrac{1}{2})\pi+\eta_j{}^c],\\ G_{j,I}&\sim\sin[x+\gamma\ln 2x-\tfrac{1}{2}(j-\tfrac{1}{2})\pi+\eta_j{}'^c],\end{aligned} \quad (34)$$

the Coulomb phase shifts being given by[23]

$$\exp 2i\eta_j{}^c=\frac{\rho_j-i\gamma}{j+\tfrac{1}{2}}\frac{\Gamma(\rho_j-i\gamma)}{\Gamma(\rho_j+i\gamma)}e^{\pi i(j+\frac{1}{2}-\rho_j)}, \quad (35)$$

$$\exp i(\eta_j{}'^c-\eta_j{}^c)=\frac{1-i\tan\pi(j+\tfrac{1}{2}-\rho_j)\coth\pi\gamma}{|1-i\tan\pi(j+\tfrac{1}{2}-\rho_j)\coth\pi\gamma|}e^{-\pi i(j+\frac{1}{2}-\rho_j)}, \quad (36)$$

where

$$\rho_j=[(j+\tfrac{1}{2})^2-\gamma^2]^{\frac{1}{2}}.$$

The phase shift of the function G_j is given by

$$\tan(\eta_j-\eta_j{}^c)=\frac{\sin(\eta_j{}'^c-\eta_j{}^c)}{(C_j/D_j)+\cos(\eta_j{}'^c-\eta_j{}^c)}. \quad (37)$$

Tables of Coulomb phase shifts and functions are being prepared and will be published in a separate paper. Some sample phase shifts are presented in Table I.

We now estimate the precision required in the calculation of the phase shifts. According to Eq. (27), an error of $\Delta\eta_j$ in η_j introduces the following error into the scattering amplitude:

$$\Delta_jf=k^{-1}\Delta\eta_je^{2i\eta_j}(j+\tfrac{1}{2})(P_{j-\frac{1}{2}}+P_{j+\frac{1}{2}}). \quad (38)$$

In any particular case it is possible to use this relation

TABLE I. Values of phase shifts for gold. The phase shift of the regular Coulomb functions $\eta_j{}^c$ are defined in Eq. (35), and the difference in phase between the irregular and regular Coulomb functions $\eta_j{}'^c-\eta_j{}^c$ in Eq. (36). $\delta_j{}^1$ and $\delta_j{}^2$ are the additional phase shifts caused by the finite nuclear charge distributions uniform, $kR=4.0$ and Gaussian, $b=2.12$, respectively. $\delta_j=\eta_j-\eta_j{}^c$ is defined by Eq. (37).

j	$\eta_j{}^c$	$\eta_j{}'^c-\eta_j{}^c$	$\delta_j{}^1$	$\delta_j{}^2$
1/2	0.40736	−1.17386	−0.85820	−0.71689
3/2	−0.23797	−0.54728	−0.27143	−0.18795
5/2	−0.53303	−0.36074	−0.07633	−0.04846
7/2	−0.72659	−0.26951	−0.01494	−0.01064
9/2	−0.87098	−0.21523	−0.00199	−0.00199
11/2	−0.98623	−0.17918	−0.00017	−0.00030
13/2	−1.08218	−0.15350	−0.00001	−0.00004
15/2	−1.16438	−0.13426	−0.00000	−0.00000
17/2	−1.23628	−0.11931	−0.00000	−0.00000

[23] N. F. Mott and H. S. W. Massey, *The Theory of Atomic Collisions* (Oxford University Press, Oxford, 1952), second edition, p. 79.

to get a fairly accurate estimate of the error in the differential cross section. For simplicity, however, we shall make some crude approximations in estimating the errors. For the charge distributions considered in the present calculations the greatest errors occur in the first few phase shifts. We therefore estimate the total error in $|f|$ to be given by a small multiple m of the error arising from $\Delta\eta_{\frac{1}{2}}$:

$$\Delta|f|=mk^{-1}|\Delta\eta_{\frac{1}{2}}|E(\theta), \tag{39}$$

where m is of the order 2 or 3, and $E(\theta)$ is a factor of order 1 which decreases to zero at $\theta=\pi$. Analysis of the quantity $(P_{j-\frac{1}{2}}+P_{j+\frac{1}{2}})$ exactly for small j and asymptotically for large j shows that a suitable form for $E(\theta)$ is $\cos\frac{1}{2}\theta$. This gives for the error in the differential cross section

$$\frac{\Delta(d\sigma/d\Omega)}{d\sigma/d\Omega}=\frac{2m|\Delta\eta_{\frac{1}{2}}|}{k(d\sigma/d\Omega)^{\frac{1}{2}}}. \tag{40}$$

It is seen that the fractional error tends to be greatest where the cross section is least.

For the purpose of comparison with the present experiments it is generally sufficient to require that the relative error in the calculated cross section be less than 10 percent at the largest angle compared. Since the differential cross section decreases rapidly with increasing angle, the relative error at smaller scattering angles will then be quite negligible. We therefore require

$$|\Delta\eta_{\frac{1}{2}}|<0.02k(d\sigma/d\Omega)_{\min}{}^{\frac{1}{2}}. \tag{41}$$

Equation (41) has two interpretations: given the cross section approximately, it tells us how accurately the phase shifts must be calculated; or when (as in practice) we know $|\Delta\eta_{\frac{1}{2}}|$, it tells us roughly the limit of the reliability of our calculations. In the present calculations we have estimated $|\Delta\eta_{\frac{1}{2}}|$ to be smaller than 0.0002 radian, based on the operations involved in obtaining $\eta_{\frac{1}{2}}$; accordingly our calculations should be sufficiently accurate whenever $k(d\sigma/d\Omega)^{\frac{1}{2}}>0.01$.

There is some empirical evidence that this estimate of the error may be too pessimistic. This is provided by the calculations for exponential and Gaussian charge distributions which yield nearly straight lines for $\log(d\sigma/d\Omega)$ *vs* θ plots. These curves continue to be linear in a region where, according to Eq. (40) and the estimate $|\Delta\eta_{\frac{1}{2}}|=0.0002$ radian, the error should be comparable in magnitude to the cross section itself! If the error were actually as large as predicted by Eq. (40), the curves should have a tendency to level off at large angles.

There are two main sources of error in the present calculation. The first is the lack of accuracy of the Coulomb functions at the fitting-on radius, due to their calculation by means of a series expansion about the origin. Cancellations which occur in the summing of the series make the final sum have a greater relative error than any of the individual terms. This error can be reduced only by computing the terms more accurately; such calculations are now in progress. The second source of error is the wave function integration. This error can be reduced by using a smaller interval or by improving the accuracy of each integration step. These two sources of error contribute about equally to the phase shift errors $\Delta\eta_j$.

4. Scattering Amplitude Series

In this section we present a new method for summing the scattering amplitude series. In previous calculations, it has been the practice to calculate first the Coulomb scattering amplitude, Eq. (27) with phase shifts given by Eq. (35), and then the corrections to it due to the finite nuclear size:

$$f=f_c+(f-f_c), \tag{42}$$

where

$$f-f_c=\frac{1}{2ik}\sum(\exp 2i\eta_j-\exp 2i\eta_j{}^c)(j+\tfrac{1}{2})(P_{j-\frac{1}{2}}+P_{j+\frac{1}{2}}). \tag{43}$$

Since $(\eta_j-\eta_j{}^c)$ approaches zero with increasing j, the series (43) converges quite rapidly even though η_j and $\eta_j{}^c$ do not individually approach zero. One sees from the Born approximation[3] that at high energies and large angles the scattering amplitude f is much smaller in magnitude than the Coulomb scattering amplitude f_c. This implies that there is almost complete cancellation between the two terms of Eq. (42), and that they must both, therefore, be known to high precision. We were unable to use the published tables of Feshbach,[22] where kf_c is given to only three decimal places and at large angular intervals.

We can discover the reason for the poor convergence of the series (27) for the case of a Coulomb potential by looking at the corresponding problem in the nonrelativistic case, where the Coulomb scattering amplitude is known analytically:

$$f_{\text{N.R.}}(\theta)=\frac{\alpha}{2k\sin^2\frac{1}{2}\theta}\exp[2i\alpha\ln\sin\tfrac{1}{2}\theta+2i\bar{\eta}_0] \tag{44}$$

$$=\frac{1}{2ik}\sum_{l=0}^{\infty}(2l+1)[\exp(2i\bar{\eta}_l)-1]P_l(\cos\theta), \tag{45}$$

where

$$\bar{\eta}_l=\arg\Gamma(l+1-i\alpha), \tag{46}$$

and

$$\alpha=Ze^2/\hbar v.$$

The series (45) with the phase shifts (46) can be rearranged in form so that it closely resembles the series (27) with the phase shifts (35).[21] For our present purposes, however, it is not necessary to do this. From Eq. (44) we see that $f_{\text{N.R.}}(\theta)$ has a singularity in both magnitude and argument at $\theta=0$. This accounts for the poor convergence of the series (45). Since for large j values the relativistic phase shifts are nearly the same as the nonrelativistic ones for $l=j-\frac{1}{2}$, the rela-

tivistic series probably has a similar type of singularity. We accordingly transform $f(\theta)$ to make it less singular for small values of θ. This is accomplished by multiplying $f(\theta)$ by a function which vanishes at $\theta=0$ and then expanding the new function in a series of Legendre polynomials.

Let us represent $f(\theta)$ by

$$2ikf=\sum a_l P_l(\cos\theta). \tag{47}$$

Then the mth "reduced" series is defined by:

$$(1-\cos\theta)^m 2ikf=\sum a_l^{(m)} P_l(\cos\theta). \tag{48}$$

Using the recurrence relations for Legendre polynomials, we find that

$$a_l^{(i+1)}=a_l^{(i)}-\frac{l+1}{2l+3}a_{l+1}^{(i)}-\frac{l}{2l-1}a_{l-1}^{(i)}. \tag{49}$$

For large l, it turns out that

$$|a_l^{(i+1)}|=O(|a_l^{(i)}|/l^2), \tag{50}$$

so that after a few reductions the series converges quite rapidly. We have found three reductions ($m=3$) to be optimum for our present calculations. For gold, the results are illustrated in Table II, where the coefficients of the series in Eq. (47) are compared with those of the third reduction.

III. DISCUSSION OF THE RESULTS

To obtain the cross section for a given charge distribution at an energy $k\hbar c$ we must use in Eq. (29) the corresponding dimensionless function $\rho(x)$, x being the radial coordinate measured in units of $k^{-1}=\lambda\!\!\!^{-}$. Equations (21) and (22), together with Eq. (29), then present the scattering problem in dimensionless form, with $kf(\theta)$ as a dimensionless scattering amplitude. The energy $k\hbar c$ thus enters the calculation in two ways: first, in the determination of the radial scale of $\rho(x)$; second, in the absolute magnitude of the cross section. For another energy $k'\hbar c$, this particular $\rho(x)$ corresponds to a physical charge distribution whose dimensions are altered by a factor k/k', and whose cross section is altered by a factor $(k/k')^2$. In the following discussion the term "shape" refers to the various analytic forms used for $\rho(x)$, and "size" refers to the value of the radial parameter involved.

We have considered the following shapes:

exponential, $\rho(x)=\rho_0 e^{-x/a}$;
Gaussian, $\rho(x)=\rho_0\exp[-(x/b)^2]$;
uniform, $\rho(x)=\rho_0$, $x<kR$, $=0$, $x>kR$;
smoothed uniform, $\rho=\rho_0[1+e^{K(x-c)}]^{-1}$;
wine-bottle, $\rho=\rho_0(1+(x/d)^4)[1+e^{K(x-c)}]^{-1}$.

Most of the calculations reported here are for gold ($Z=79$, $\gamma=Ze^2/\hbar c=0.5765$). A few are for copper ($Z=29$, $\gamma=0.2116$) and for aluminum ($Z=13$, $\gamma=0.09486$).

TABLE II. Coefficients of the Legendre series for the Coulomb scattering amplitude. a_l are those for the original series in Eq. (47), and $a_l^{(3)}$ are the third reduced coefficients defined by Eq. (49).

l	Rea_l	Ima_l	Re$a_l^{(3)}$	Im$a_l^{(3)}$
0	0.68608	0.72753	−0.40271	0.64187
1	2.46374	−0.18893	0.46429	−0.39809
2	3.22837	−3.54238	0.28802	−0.66577
3	1.92010	−6.59828	−0.48598	0.40511
4	−0.38223	−8.89930	0.10826	0.02838
5	−3.19735	−10.44940	0.01935	−0.00448
6	−6.26093	−11.32514	0.00547	−0.00298
7	−9.41473	−11.61261	0.00194	−0.00162
8	−12.55937	−11.39191	0.00078	−0.00091
9	−15.63076	−10.73364	0.00034	−0.00053
10	−18.58706	−9.69883	0.00016	−0.00032
11	−21.40100	−8.33997	0.00007	−0.00020
12	−24.05511	−6.70216		
13	−26.53869	−4.82425		
14	−28.84572	−2.73981		

5. Comparison with the First Born Approximation

The differential cross section predicted by the first Born approximation is

$$\frac{d\sigma}{d\Omega}=\left(\frac{\gamma}{2k}\right)^2\frac{\cos^2\tfrac{1}{2}\theta}{\sin^4\tfrac{1}{2}\theta}\left|\int\rho(x)e^{i\mathbf{q}\cdot\mathbf{x}}d^3x\right|^2,$$

where $|\mathbf{q}|=2\sin\tfrac{1}{2}\theta$, and ρ, as in Eq. (30), has unit volume integral.[3] The scattering amplitude is real. For simpler shapes the "form factor" $F=\int\rho(x)\exp(i\mathbf{q}\cdot\mathbf{x})d^3x$ has the following forms:

exponential, $F=(1+q^2a^2)^{-2}$;
Gaussian, $F=\exp(-q^2b^2/4)$;
uniform, $F=3(\sin qkR-qkR\cos qkR)/(qkR)^3$.

The cross sections for the first two shapes are, on a semilog plot, smooth functions of θ; for the uniform shape, on the other hand, F has zeros (where $qkR=\tan qkR$) and the cross section is a wildly varying function of θ. In Figs. 1, 2, and 3 the dashed curves are the Born approximation cross sections for a uniform shape $kR=5.4$, exponentials $a=0.91$ and $a=1.06$, and Gaussians $b=2.12$ and $b=3.4$, respectively.

The cross sections obtained from the phase-shift analysis are, for gold, usually considerably different from the first Born approximation cross sections.[4] For the uniform shape, the first zero of the Born cross section appears only as a slight undulation, and the second zero barely as a minimum, which is shifted to a slightly smaller angle. In Fig. 1 is shown the cross section for the uniform shape $kR=5.4$, together with the cross section for the same shape in copper, suitably normalized to have the same Born cross section. For copper the agreement with the Born approximation is much better than for gold, as is to be expected.

The results of the phase-shift analysis for the ex-

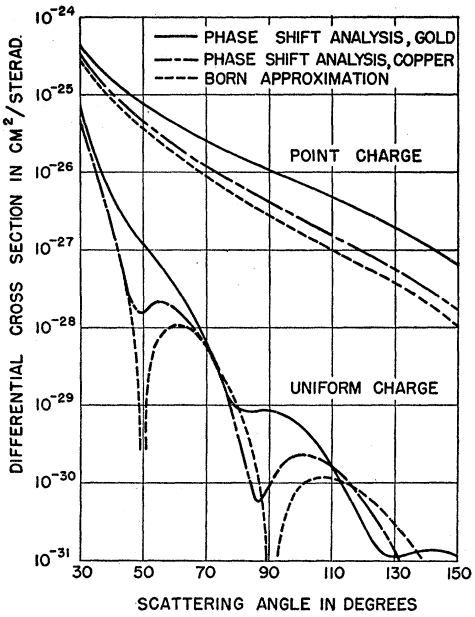

FIG. 1. Differential cross sections at 150 Mev for scattering by a point charge and by the uniform charge distribution $kR=5.4$, for gold and copper. The cross sections for copper have been multiplied by a factor that makes their first Born approximations the same as those for gold.

ponential shape are shown in Fig. 2. The cross section is a smooth function of θ, but has a considerably greater over-all slope than the Born cross section. Thus fitting experimental results with the phase-shift analysis predicts a smaller nucleus than fitting with the Born approximation.

For the Gaussian shape with $b=2.12$, the phase-shift

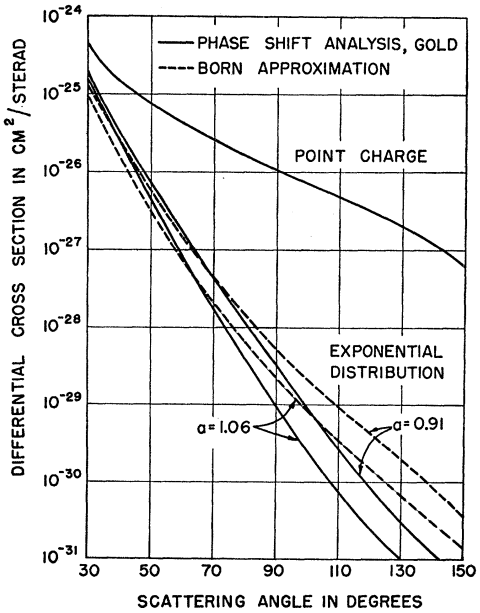

FIG. 2. Cross sections at 150 Mev for scattering by the exponential shapes $a=0.91$ and $a=1.06$, for gold.

analysis cross section, shown in Fig. 3, is almost identical with the Born cross section, whereas for $b=3.4$ it slopes less steeply. The phase-shift analysis results for the exponential and uniform shapes could be understood, as suggested previously,[4] in terms of the increase in wave number as the electron entered the attractive field of the nucleus. The results for Gaussian shapes, however, lie if anything in the opposite direction, so that such a simple interpretation is ruled out.

The difference between the phase-shift analysis and the first Born approximation is even more pronounced in the scattering amplitude, which in the phase-shift analysis is, of course, complex. In Figs. 4 and 5 we exhibit this complex behavior by making polar plots of $\log_{10}|f(\theta)|$ *versus* argument $(f(\theta))$. The values $\theta=30°$, 50°, 70°, $\cdots$ are indicated on each curve. In Fig. 4 are

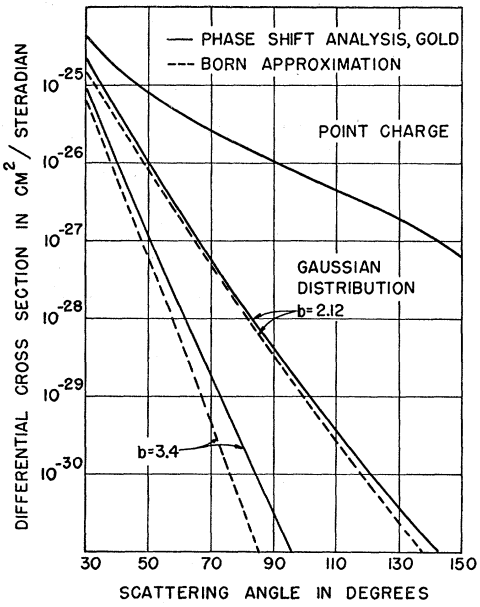

FIG. 3. Cross sections at 150 Mev for scattering by the Gaussian shapes $b=2.12$ and $b=3.4$, for gold.

the results for point scattering on Al, Cu, and Au, and for the uniform shape $kR=5.4$, in Cu and Au. In the first Born approximation the scattering amplitude lies along the horizontal axis. For a cross section with zeros it crosses the origin. The exact point-scattering amplitude is almost real for Al, and becomes more and more complex as Z increases. The scattering amplitude for the uniform shape $kR=5.4$ is for Cu a flattened spiral whose major axis is at about 30° to the horizontal axis and the Born approximation amplitude, while for Au it is an unflattened spiral. The filling in of the zeros in the Born approximation cross section and the fact that the exact scattering amplitude is complex are thus the same phenomenon. In Fig. 5 are scattering amplitudes for a number of charge shapes in gold. We find that for a given shape the polar plot is remarkably independent of size. For the Gaussian shape, for instance, the curves

for $b=3.4$ and $b=2.12$ are almost the same. The difference in the corresponding cross sections occurs because values of θ on the $b=3.4$ curve are shifted relative to the corresponding values of θ on the $b=2.12$ curve. Another peculiar fact is that the exponential shape $ka=0.91$ and the Gaussian shape $kb=2.12$ have very different scattering amplitudes but almost identical cross sections.

The first Born approximation cross sections are thus of little value in suggesting the correct sizes to use when fitting the data. The fact that the phase-shift analysis yields cross sections which are always smoother functions of θ means that a much wider range of shapes gives a tolerable fit with experiment than was suggested by the use of the Born approximation.

6. Interpolation

It is useful to be able to estimate the effect on the cross section of changing the size slightly, without doing a large number of trial calculations. For the smooth cross sections yielded by the Gaussian shapes, it is possible to interpolate by fitting cross sections at a particular value of θ to a polynomial in the size parameter. Since we usually need only relative cross sections, our procedure is to fit the ratio of the values of $\log_{10}[d\sigma(\theta)/d\Omega]-\log_{10}[d\sigma(\theta')/d\Omega]$ given respectively by the phase-shift analysis and the first Born approximation to a polynomial in the size parameter b. Extrapolating in this way from cross sections for $b=3.4$ and $b=2.69$ gives a cross section for $b=2.12$ which by later comparison with the phase-shift analysis we have found to be accurate to about 2 percent. The cross section for the Gaussian shape $b=3.05$ shown in Fig. 10 was obtained by this method.

Such a method is clearly unsuitable for cross sections given by uniform shapes. For these we make use of the fact that the "form factor" $\mathfrak{F}(\theta,kR)$ defined in terms of the phase-shift analysis cross sections by

$$\{\mathfrak{F}(\theta,kR)\}^2=\{d\sigma(\theta)/d\Omega\}/\{d\sigma(\theta)/d\Omega\}_{\text{point}}$$

has properties very similar to those of the form factor $F(\theta,kR)$ of the first Born approximation.[24] There, F is a function of $2kR\sin\frac{1}{2}\theta$ whose analytic form is the same for all kR (see the beginning of Sec. 5), so that $F(\theta,kR)$ and $F(\theta',kR')$ for two sizes have equal values when $kR'\sin\frac{1}{2}\theta'=kR\sin\frac{1}{2}\theta$. Hence in the first Born approximation the cross sections for all sizes can be obtained from a knowledge of the point cross section and the form factor F for one size. In the case of the phase-shift analysis we find that the two angles defined by

$$\mathfrak{F}(\theta,5.4)=\mathfrak{F}(\theta',4.0)$$

are connected by the relation $\sin\frac{1}{2}\theta/\sin\frac{1}{2}\theta'=\text{constant}\pm 4$ percent over the angular range 30° to 150°. The "constant" is roughly $(4.0/5.4)^{0.8}$. Hence to within 4 percent $\mathfrak{F}$ can be written $\mathfrak{F}(g(kR)\sin\frac{1}{2}\theta)$, and, as with the first Born approximation, is (approximately) a universal function independent of size. When obtained by the phase-shift analysis for a particular size it can be used for other slightly different sizes. Of the family of uniform shapes shown in Fig. 6, the $kR=4.0$ curve was obtained by the phase-shift analysis, and the rest by this interpolation method, as was also the uniform $kR=5.8$ curve of Fig. 10.

[24] This was suggested to us by Dr. McIntyre.

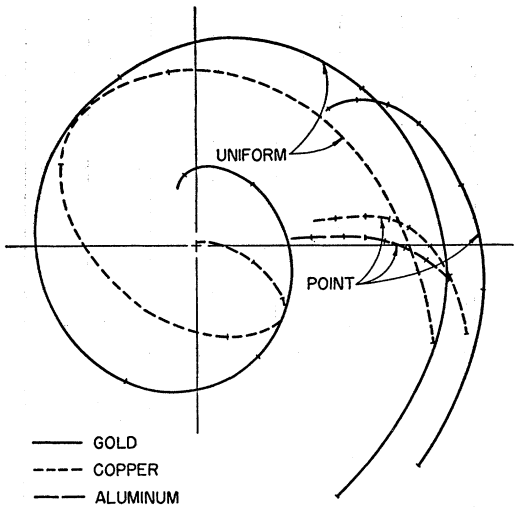

FIG. 4. Plots of $\log_{10}|f(\theta)|$ *versus* $\arg f(\theta)$, in polar coordinates, for point scattering in gold, copper, and aluminum, and for the uniform shape $kR=5.4$ in gold and copper. The values $\theta=30°$, 50°, 70°, ··· are indicated on each curve.

7. Comparison with Other Calculations

Calculations of other authors seem to confirm our results fairly well. Numerical errors have been discovered in the published work of Parzen.[9,10] In any case it seems physically rather unlikely that the phase-shift

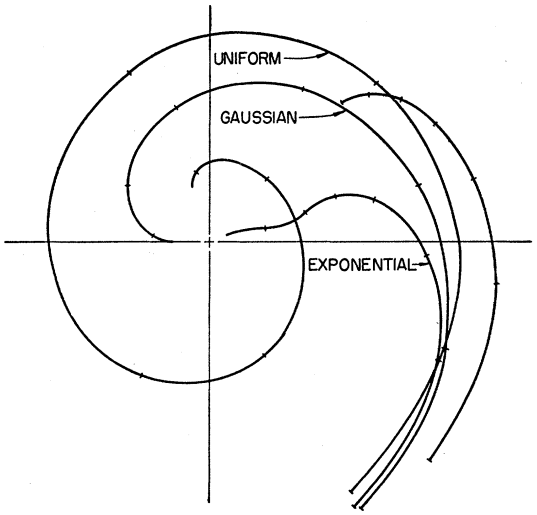

FIG. 5. Plots of $\log_{10}|f(\theta)|$ *versus* $\arg f(\theta)$, in polar coordinates, for a point charge and the following shapes, all for gold: uniform, $kR=5.4$; exponential, $a=0.91$; Gaussian, $b=2.12$.

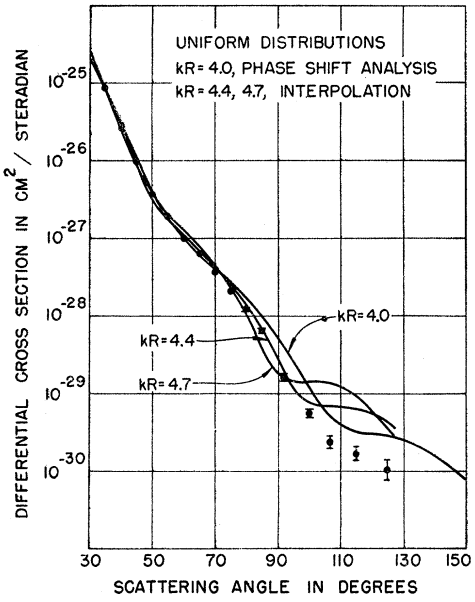

FIG. 6. Cross sections at 125 Mev for scattering by three uniform shapes, $kR=4.0$, 4.4, 4.7, for gold, together with the experimental data. All have been normalized to the same value at 35°. The ordinate scale refers to the $kR=4.0$ curve. This was obtained by the phase-shift analysis, the other two by interpolation. The nuclear radii corresponding to these shapes have r_0 values of 1.09×10^{-13} cm, 1.19×10^{-13} cm, 1.27×10^{-13} cm, where $R=r_0A^{\frac{1}{3}}$. From Eq. (40) the estimated error in the $kR=4.0$ curve is 10 percent when $d\sigma(\theta)/d\Omega\cong3\times10^{-30}$ cm² per steradian, i.e., when $\theta\cong120°$. For θ larger than 120° the error is larger.

analysis cross sections should be many times the first Born cross sections. A phase-shift analysis in which the phase shifts were obtained by the W.K.B. approximation has been made by Baranger.[11] The cross section she obtains for the uniform shape $kR=5.0$, in mercury, $Z=80$, resembles closely our cross section for the uniform shape $kR=5.4$ in gold, although its plateau (corresponding to the Born approximation second zero) is a little higher than that of our curve. Brenner, Brown, and Elton[12] have obtained phase shifts by numerical integration. Their cross section for the uniform shape $kR=4.4$ in mercury seems to agree very closely with our uniform $kR=4.4$ shape in gold. For the uniform $kR=5.28$ shape, however, their cross section tends to be rather larger than ours (obtained by interpolation from $kR=5.4$) at large angles. Their results for a smoothed uniform shape, with a slightly different analytic function from that we have used, check very closely our conclusions on this shape in Sec. 8. Both Baranger, and Brenner, Brown, and Elton, however, have used Feshbach's values of the Coulomb scattering amplitude[22] for mercury, $Z=80$. Results for $Z=80$ should not differ appreciably from results for $Z=79$, but, as we point out in Sec. 4, Feshbach's values are probably not accurate enough to yield reliable cross sections at large angles.

8. Cross Sections for Gold at 125 Mev

Experimental results for gold at 125 Mev are included in Figs. 6, 7, and 8. They are part of the new data obtained recently by Hofstadter's group.[25] They indicate a cross section which decreases steadily with θ (on this semilog plot) out to about 120°, with a slight dip at about 60°. We have found a wide variety of charge shapes all of which give cross sections having roughly this character, although these cross sections do not all fit the experimental results equally well. Since it appears that a comparison with experiment at several

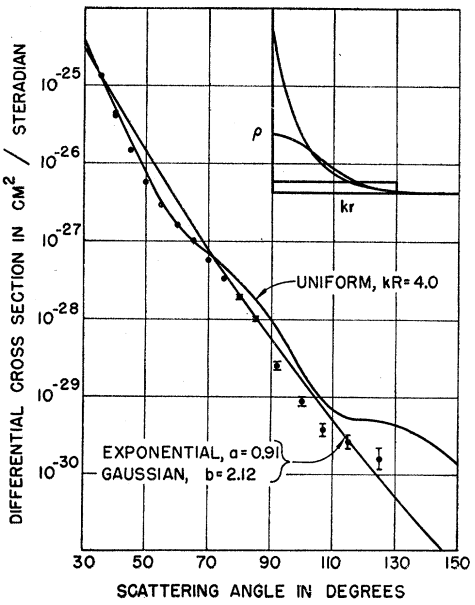

FIG. 7. Cross sections at 125 Mev for scattering by the uniform shape $kR=4.0$, the exponential $a=0.91$, and the Gaussian $b=2.12$, for gold, together with the experimental data. When all are normalized to the same value at 35° the cross sections for the Gaussian and exponential shapes coincide. The ordinate scale refers to the Gaussian shape. The rms radii of the three shapes are, respectively, 3.10λ̄, 3.16λ̄, and 2.60λ̄ Inset are scale drawings of ρ.

energies is required to obtain the charge distribution accurately, we want in this paper only to give the trend that our present calculations suggest.

In Fig. 6 the cross sections of a family of uniform charge distributions are plotted together with the experimental results. That for $kR=4.0$ is obtained from our phase-shift analysis, the others by the interpolation method given in Sec. 6. Since the measured cross section is only relative, the scale of the interpolated curves has been altered so that they have the same value at 35° as the cross section for $kR=4.0$, and the

[25] The data with which we compared our calculations as they were made were means of the earlier published cross sections (see reference 1) and later unpublished ones, all obtained before improvements in the experimental apparatus enabled Hofstadter's group to obtain their new and more accurate data. These means of the old data agreed very well with the new data, although their probable error was of course much larger. We are grateful for Professor Hofstadter's permission to quote the new results before their publication.

experimental 35° point has been plotted here also. It seems from Fig. 6 that it will be difficult to fit both the general slope in the range 35°–80°, and the fact that there is no plateau, with a uniform charge distribution.

Figure 7 contains the cross sections for the exponential $a=0.91$, Gaussian $b=2.12$, and uniform $kR=4.0$ charge distributions, normalized at 35°, together with the experimental results. It is remarkable that over the whole range of θ used, the cross sections for the first two shapes are so closely proportional that in this figure we are unable to distinguish between them. Indeed, for angles less than 90° the cross sections of all three shapes are not very different. As regards comparison with experiment, it is seen that the cross sections of the exponential and Gaussian do decrease steadily with angle, but they have no dip at 60°. A shape having some of the features of each of those of Fig. 7 seems to be indicated. The root-mean-square radius may be taken as a measure of the relative size

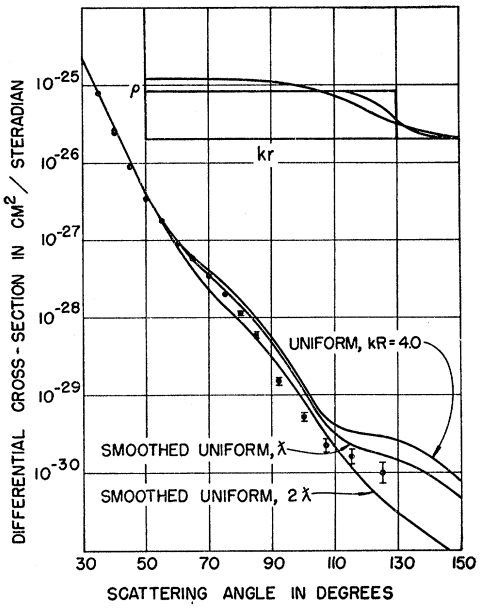

FIG. 8. Cross sections at 125 Mev for scattering by the uniform shape $kR=4.0$ and two smoothed uniform shapes: $K=4.40$, $c=3.86$; and $K=2.20$, $c=3.51$, for gold, together with the experimental data. The "smoothing distances" of the second and third shapes are λ̄ and 2λ̄ at this energy. The rms radii of the three shapes are all 3.10λ̄. Inset are scale drawings of ρ.

of these charge distributions. In units of k^{-1} it is respectively 3.16, 2.60, and 3.10 for these three shapes.

The smoothed uniform shape represents a charge distribution intermediate between uniform and exponential. The two cross sections in Fig. 8 are for smoothed uniform shapes having the same rms radius as the uniform $kR=4.0$ distribution. They have smoothing distances of 1 and 2, in units of k^{-1}. (We define smoothing distances as the distance over which ρ decreases from 0.9 $\rho(0)$ to 0.1 $\rho(0)$.) The shape with a smoothing distance of 1, that is λ̄, has a cross section almost the same as that of the uniform shape, whereas the shape with a smoothing distance of 2 (i.e., 2λ̄) has a cross section which approaches that of an exponential. It thus appears that at this energy only smoothed uniform shapes with smoothing distances between λ̄ and 2λ̄ have cross sections distinctly different from those of uniform or exponential. It seems likely that by appropriately choosing c and K a cross section can be obtained which will have the features shown by the experimental one. Such a shape would have about the same rms radius as those of Fig. 8.[25a]

As a shape in which charge is dispersed towards the edge of the nucleus we have considered the "wine-bottle."[26] As Fig. 9 shows, such a shape, with $d=c$, having the same rms radius as the uniform $kR=4.0$, and a maximum charge density 1.46 times its central density, has a cross section almost identical with the uniform $kR=4.0$ shape.

The experimental data at 125 Mev can probably be fitted with quite a range of charge distributions. The situation is much more definite, however, if a fit is made at two energies. For example, Fig. 10 shows the cross sections at 180 Mev given by the Gaussian and uniform nuclear charge distributions whose cross sections at 125 Mev are shown in Fig. 7. These were obtained by the interpolation methods described in Sec. 6. Experimental results at 180 Mev should be able to discriminate between them.

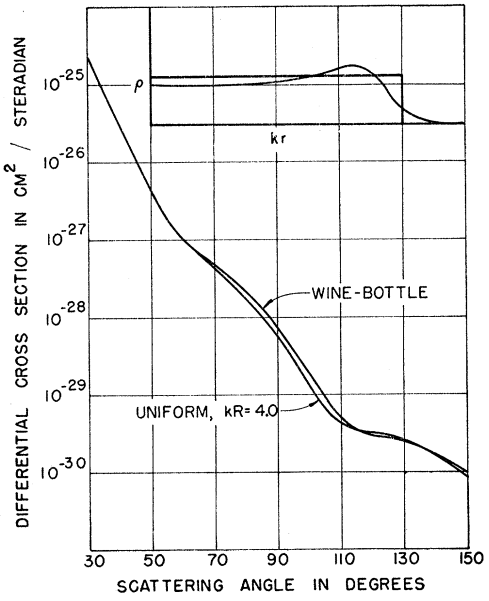

FIG. 9. Cross sections at 125 Mev for scattering by the uniform shape $kR=4.0$ and the "wine-bottle" shape with $K=5.45$ and $c=d=3.67$, for gold. These shapes have the same rms radius, and the second has a maximum charge density 1.46 times the central density. Inset are scale drawings of ρ.

[25a] *Footnote added in proof.*—Later calculations indicate that the rms radius will be a little larger (about 5 or 10 percent) than those of the charge distributions of Fig. 8.

[26] Such a charge distribution has been suggested by E. Feenberg, Phys. Rev. **59**, 593 (1941).

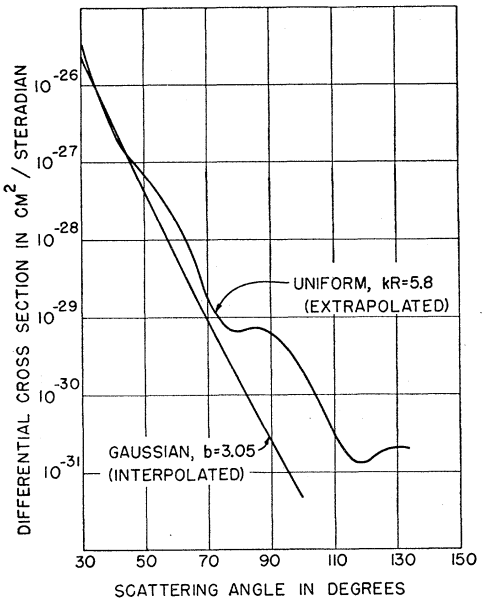

FIG. 10. Cross sections at 180 Mev for scattering by the Gaussian and uniform nuclear charge distributions whose cross sections at 125 Mev are shown in Fig. 7. At 180 Mev they correspond to the uniform $kR=5.8$ and Gaussian $b=3.05$ shapes. The cross sections were obtained by the interpolation methods of Sec. 6.

9. Conclusions

It seems likely that the experimental results in gold at 125 Mev, or at any one energy, can be fitted by quite a range of charge distributions, and that comparisons between theory and experiment at several energies will be needed to obtain a unique result. From the few calculations we have already made it appears that a smoothed uniform charge distribution with smoothing distance a little greater than $\lambda\!\!\!^{-}$ (for terminology, see Sec. 8) could fit the 125 Mev data. It would have a root-mean-square radius about equal to that of a uniform distribution with radius $R=1.1\times10^{-13}A^{\frac{1}{3}}$ cm.[25a] But we have tried only a small sample of all conceivable charge distributions, and it may well be possible to find another one quite different from this which also fits the data at 125 Mev.

We wish to thank Professor L. I. Schiff for his advice on all phases of the work, and Professor R. Hofstadter and Dr. J. A. McIntyre for many stimulating and fruitful conversations. Advice on programming for the Stanford I.B.M. Card-Programmed Calculator by Professor J. G. Herriot and Mr. J. Carter, and instruction in its operation by Mrs. H. Van Heusen, are much appreciated.

APPENDIX

1. Comparison of the Present Treatment of the Dirac Equation with Those of Other Authors

Most previous treatments of the electron-scattering problem are based on the separation of the Dirac equation given by Darwin.[27] It seems worth while to show here the connection between Darwin's treatment and ours.

In place of (1), Darwin uses

$$(-\boldsymbol{\alpha}'\cdot\mathbf{p}c-\beta'mc^2+V)\psi'=E\psi', \tag{A1}$$

where[15]

$$\alpha'_i=\rho_1\sigma_i,\quad \beta'=\rho_3. \tag{A2}$$

The two representations are connected by

$$-\alpha_i'=U^{-1}\alpha_iU,\quad -\beta'=U^{-1}\beta U, \tag{A3}$$

where

$$U=U^{-1}=(1/\sqrt{2})(\rho_1-\rho_3). \tag{A4}$$

The partial wave solutions of (A1) take the form

$$\psi_n'=r^{-1}\begin{pmatrix}-i\mathfrak{F}_n(r)\chi_{n+\frac{1}{2}}{}^2\\ \mathfrak{G}_n(r)\chi_{n+\frac{1}{2}}{}^1\end{pmatrix}(n=0,\,1,\,2,\,\cdots), \tag{A5}$$

$$\psi_{-n-1}'=r^{-1}\begin{pmatrix}-i\mathfrak{F}_{-n-1}(r)\chi_{n-\frac{1}{2}}{}^1\\ \mathfrak{G}_{-n-1}(r)\chi_{n-\frac{1}{2}}{}^2\end{pmatrix}(n=1,\,2,\,3,\,\cdots), \tag{A6}$$

where the two-component functions χ^1 and χ^2 are given by Eq. (13). The radial functions $\mathfrak{F}_n$ and $\mathfrak{G}_n$ satisfy

$$\begin{aligned}&\frac{d\mathfrak{G}_n}{dr}-\frac{(n+1)}{r}\mathfrak{G}_n+\frac{(E-V+mc^2)}{\hbar c}\mathfrak{F}_n=0,\\ &\frac{d\mathfrak{F}_n}{dr}+\frac{(n+1)}{r}\mathfrak{F}_n-\frac{(E-V-mc^2)}{\hbar c}\mathfrak{G}_n=0.\end{aligned} \tag{A7}$$

$\mathfrak{F}_{-n-1}$, $\mathfrak{G}_{-n-1}$ satisfy the same equations with n replaced by $-n-1$. Comparing Eq. (A7) with Eq. (18), we find that in the limit $m\to0$

$$\begin{aligned}\mathfrak{G}_n&=\mathfrak{F}_{-n-2}=G_{n+\frac{1}{2}},\\ \mathfrak{F}_n&=-\mathfrak{G}_{-n-2}=F_{n+\frac{1}{2}}.\end{aligned} \tag{A8}$$

Transforming Eqs. (A5) and (A6) to the representation used in the present paper, we obtain

$$\begin{pmatrix}\phi_{j,\frac{1}{2}}\\ 0\end{pmatrix}=\frac{1}{\sqrt{2}}(\psi_n-i\psi_{-n-2}), \tag{A9}$$

$$\begin{pmatrix}0\\ \chi_{j,\frac{1}{2}}\end{pmatrix}=\frac{1}{\sqrt{2}}(\psi_n+i\psi_{-n-2}). \tag{A10}$$

The states (A5) and (A6) have definite parity while (A9) and (A10) do not.

The index n in Eqs. (A5) and (A6) seems to have been selected because it is the order of the spherical harmonics in the third and fourth components of ψ_n' and ψ_{-n-1}' and not because of its connection with any particular quantum number. An alternative is to use the quantum number $k(=\pm(j+\frac{1}{2}))$, defined by the operator

$$\hbar k=\beta'(\boldsymbol{\sigma}'\cdot\mathbf{L}+\hbar). \tag{A11}$$

[27] C. G. Darwin, Proc. Roy. Soc. (London) **A118**, 654 (1928).

This notation has been used by Acheson.[6] His radial functions $f_{\pm\kappa}$ and $g_{\pm\kappa}$ are related to those of Darwin as follows:

$$f_\kappa=\mathfrak{F}_{\kappa-1}, \quad g_\kappa=\mathfrak{G}_{\kappa-1}(\kappa=k=j+\tfrac{1}{2}), \tag{A12}$$

$$f_{-\kappa}=\mathfrak{F}_{-\kappa-1}, \quad g_{-\kappa}=\mathfrak{G}_{-\kappa-1}(\kappa=-k=j+\tfrac{1}{2}). \tag{A13}$$

With this notation the radial equations become

$$\begin{aligned}\frac{dg_{\pm\kappa}}{dr}\mp\frac{\kappa}{r}g_{\pm\kappa}+\frac{(E-V+mc^2)}{\hbar c}f_{\pm\kappa}=0,\\ \frac{df_{\pm\kappa}}{dr}\pm\frac{\kappa}{r}f_{\pm\kappa}+\frac{(E-V-mc^2)}{\hbar c}g_{\pm\kappa}=0.\end{aligned} \tag{A14}$$

We have not used this notation because the partial waves (A9) and (A10) are not eigenfunctions of k.

2. Calculation of Coulomb Functions

Mott and Massey have given the Coulomb functions in terms of confluent hypergeometric functions.[23] We use instead the more rapidly convergent series solution given by Elton:[28]

$$\begin{aligned}G_j&=x^{s_j}N_j\sum_{m=0}^{\infty}a_m^{(j)}x^m,\\ F_j&=x^{s_j}N_j\sum_{m=0}^{\infty}b_m^{(j)}x^m,\end{aligned} \tag{A15}$$

where

$$s_j=\pm\rho_j=\pm[(j+\tfrac{1}{2})^2-\gamma^2]^{\frac{1}{2}}.$$

The positive sign gives the regular solution, and the negative sign the irregular solution. The coefficients of the series are given by

$$a_0=1, \quad b_0=\gamma/(s_j+j+\tfrac{1}{2}), \tag{A16}$$

together with the recurrence relations:

$$\begin{aligned}m(m+2s_j)a_m^{(j)}&=-\gamma a_{m-1}^{(j)}\\ &\quad-(s_j+m+j+\tfrac{1}{2})b_{m-1}^{(j)},\\ m(m+2s_j)b_m^{(j)}&=-\gamma b_{m-1}^{(j)}\\ &\quad+(s_j+m-j-\tfrac{1}{2})a_{m-1}^{(j)}.\end{aligned} \tag{A17}$$

The normalization, obtained by comparison with Mott and Massey's solutions, is

$$N_j=\frac{s_j}{|s_j|}\frac{2^{s_j}|\Gamma(s_j+i\gamma)|}{\Gamma(2s_j+1)}\left[\frac{(j+\frac{1}{2})(j+\frac{1}{2}+s_j)}{2}\right]^{\frac{1}{2}}e^{\frac{1}{2}\pi\gamma}. \tag{A18}$$

3. Numerical Integration of the Radial Dirac Equations

We use a step-by-step procedure based on derivatives rather than differences. Let y_n, y_n', y_n'', $\cdots$ be a function and its derivatives at $x=x_n$. Alternative approximate formulas, given by Milne,[29] for y_{n+1} at $x_{n+1}=x_n+h$ are

$$y_{n+1}=y_n+\tfrac{1}{2}h(y_n'+y_{n+1}'), \tag{A19}$$

$$y_{n+1}=y_n+\tfrac{1}{2}h(y_n'+y_{n+1}')+(1/12)h^2(y_n''-y_{n+1}''), \tag{A20}$$

$$y_{n+1}=y_n+\tfrac{1}{2}h(y_n'+y_{n+1}')+(1/10)h^2(y_n''-y_{n+1}'')+(1/120)h^3(y_n'''+y_{n+1}'''). \tag{A21}$$

The respective errors are of order $h^3y'''/12$, $h^5y^{(5)}/720$, $h^7y^{(7)}/100\,800$. The method can easily be extended to take more derivatives into account. We use Eq. (A20) to obtain the results of Part III.

Since Eqs. (21) are linear,[30] we may solve Eqs. (A19–A21) exactly for y_{n+1} in terms of y_n. Let y_n be a column matrix composed of $F_{j,n}$ and $G_{j,n}$

$$y_n=\begin{pmatrix}F_j\\ G_j\end{pmatrix}_n. \tag{A22}$$

Then from Eqs. (21), the derivatives of y_n can be represented by matrices acting on y_n:

$$y_n'=A_ny_n, \quad y_n''=B_ny_n, \quad y_n'''=C_ny_n. \tag{A23}$$

For example,

$$A_n=\begin{pmatrix}-(j+\frac{1}{2})/x_n & (1-v_n)\\ -(1-v_n) & (j+\frac{1}{2})/x_n\end{pmatrix}. \tag{A24}$$

The solutions of Eqs. (A19–A21) are given by

$$y_{n+1}=\left(1-\frac{h}{2}A_{n+1}\right)^{-1}\left(1+\frac{h}{2}A_n\right)y_n, \tag{A25}$$

$$y_{n+1}=\left(1-\frac{h}{2}A_{n+1}+\frac{h^2}{12}B_{n+1}\right)^{-1}\times\left(1+\frac{h}{2}A_n+\frac{h^2}{12}B_n\right)y_n, \tag{A26}$$

$$y_{n+1}=\left[1-\frac{h}{2}A_{n+1}+\frac{h^2}{10}B_{n+1}-\frac{h^3}{120}C_{n+1}\right]^{-1}\times\left[1+\frac{h}{2}A_n+\frac{h^2}{10}B_n+\frac{h^3}{120}C_n\right]y_n. \tag{A27}$$

[28] L. R. B. Elton, Proc. Phys. Soc. (London) **A66**, 806 (1953). There is a sign error in Elton's Eq. (3.14).

[29] W. E. Milne, *Numerical Solution of Differential Equations* (John Wiley and Sons, Inc., New York, 1953), pp. 76–78.

[30] When this method is applied to nonlinear differential equations y_{n+1} is obtained from y_n by an iteration procedure.

We can make some estimates of the errors involved in using this method. Inside the turning point (which is at $x \cong j$), any small errors made in an integration step will bring in a small amount of irregular function. However, in this region the regular function increases rapidly with increasing x, while the irregular function decreases rapidly. Thus, in this region, the effect of a small error tends to be damped quickly. Of course the normalization near the origin may differ from that outside the turning point because of these errors, but that does not affect the present calculations since we need only the ratio (F_j/G_j) at the fitting-on radius.

Outside the turning point the error in the phase can be estimated by replacing the Eqs. (21) by the equations

$$g'=-f, \quad f'=+g, \tag{A28}$$

which have the solutions

$$g=\cos x, \quad f=\sin x.$$

Equations (A19–A21) have the solution[31]

$$g=\cos\lambda x, \quad f=\sin\lambda x,$$

where

$$\lambda=1-h^2/12,$$
$$\lambda=1-h^4/720,$$
$$\lambda=1-h^6/100\,800,$$

respectively. The total phase error in a distance L is therefore

$$\delta\phi=h^2L/12,$$
$$\delta\phi=h^4L/720,$$
$$\delta\phi=h^6L/100\,800,$$

for the three approximations.

If we require $\delta\phi<10^{-4}$, for $L=8$ we find in the respective cases:

$$h<10^{-2}, \quad h<0.3, \quad h<1.$$

The interval that would be required using Eq. (A19) is prohibitively small. With Eq. (A20) there is more computing work at each step of the integration, but the interval is reasonable. One could not use such a large interval with Eq. (A21) as estimated here because of the variation of A_n with x. With a smaller interva Eq. (A21) may be useful in obtaining greater accuracy

[31] This was pointed out to us by Professor L. I. Schiff.

PHYSICAL REVIEW VOLUME 95, NUMBER 2 JULY 15, 1954

High-Energy Electron Scattering and Nuclear Structure Determinations. II*†‡

R. HOFSTADTER, B. HAHN,§ A. W. KNUDSEN, AND J. A. MCINTYRE
Department of Physics and W. W. Hansen Laboratories of Physics, Stanford University, Stanford, California

(Received April 1, 1954)

Elastic scattering measurements have been carried out with electrons in Au^{197} at energies of 84, 126, 154, and 183 Mev and in Pb^{208} at 84, 153, and 186 Mev. Diffraction effects are observed which appear to vary with momentum and angular position as if a fundamental parameter $p\sin(\theta/2)$ were equal to a constant for a given diffraction feature. Such a behavior would be predicted by the Born approximation. A comparison of the scattering in Au^{197} and Pb^{208} suggests that inelastic scattering does not materially influence the scattering curves presented. The appearance of diffraction effects indicates a model more nearly uniform in charge density than early tentative conclusions based on Born approximation calculations.

I. INTRODUCTION

IN the first paper of this series with the above title[1] experimental electron scattering curves were presented for several materials at 125 Mev. Elastic profiles were shown, the apparatus was described, various checks on the experimental information were discussed, and other relevant information was given. A preliminary attempt to explain the at-that-time unexpected absence of prominent diffraction peaks was made in terms of a first-order Born approximation calculation for various nuclear charge distributions.[1,2] These approximate calculations led to a tentative interpretation which indicated a smooth decrease of charge density from the center to the outer regions of heavy nuclei such as gold and lead. It must be borne in mind that the conventional values of nuclear radius (for example, root-mean-square values) were retained in this interpretation.

It has recently been shown by Yennie, Wilson, and Ravenhall[3] that an accurate phase shift calculation for

* The research reported in this document was supported jointly by the U. S. Office of Naval Research and the U. S. Atomic Energy Commission, and by the U. S. Air Force through the Office of Scientific Research of the Air Research and Development Command.
† Aided by a grant from the Research Corporation.
‡ This material was presented in part at the New York Meeting of the American Physical Society in January, 1954 [Phys. Rev. 94, 773 (1954)].
§ Visiting Post Doctoral Research Fellow of the Schweizerische Arbeitsgemeinschaft in Mathematik und Physik, Switzerland.
[1] Hofstadter, Fechter, McIntyre, Phys. Rev. 92, 978 (1953). We shall refer to this paper as I.
[2] L. I. Schiff, Phys. Rev. 92, 988 (1953).
[3] Yennie, Wilson, and Ravenhall, Phys. Rev. 92, 1325 (1953).